Nature Environment and Pollution Technology
An International Quarterly Scientific Journal

p-ISSN: 0972-6268
(Print copies up to 2016)
e-ISSN: 2395-3454

Vol. 21 | No. 2 | pp. 683-689 | 2022

Original Research Paper

https://doi.org/10.46488/NEPT.2022.v21i02.028

Open Access Journal

Distinguished Ni(II) Capture with Rapid and Superior Capability Using Biochar: Behavior and Mechanism

Y. Wang*, S. Zhang and Y. Zheng*†**

*Shaoxing Huaxia Printing and Dyeing Co. Ltd, Shaoxing, Zhejiang 312000, People's Republic of China

**Shaoxing Quality Technical Supervision and Testing Institute, Shaoxing, Zhejiang 312000, People's Republic of China

†Corresponding author: Y. Zheng; zhenyinhua2021@163.com

Nat. Env. & Poll. Tech.
Website: www.neptjournal.com

Received: 10-06-2021
Revised: 29-07-2021
Accepted: 26-08-2021

Key Words:
Biochar
Interaction effect
Ni(II)

ABSTRACT

Batch experiments were used to study the interaction mechanism of Ni(II) with biochar as a function of solution pH, contact time, initial concentrations, reaction temperature, and the addition of humic compounds. The results indicate that Ni(II) can be interacted with biochar by a compound mechanism under different environmental conditions. It is suggested that outer-sphere surface complexes at low pH are transformed into inner-sphere surface complexes and surface precipitates are formed at pH 8.89 or 10.18. The combined macroscopic and microscopic insights provide additional details regarding the mobility, fate, and risk of Ni(II) in a practical aquatic environment, as well as the natural purification of metals in ecological environments.

INTRODUCTION

Toxic heavy metals are becoming an increasingly important issue in water bodies and soil remediation, because of their mobility, toxicity, and difficult biodegradation. Nickel (Ni) is one of the most widespread contaminants, especially for ecosystem stability and public health sake (Malkoc 2006). Conventional methods of Ni(II) removal include chemical redox, precipitation, ion exchange, membrane separation, filtration, and electrochemistry. Aside from these suboptimal methods, adsorption techniques are more commonly used to remove heavy metal ions from water due to their low cost, ease of availability, and high removal efficiency.

Biochar is a carbon-rich, porous solid produced by the thermal decomposition of bioenergy feedstocks (e.g., grass, crop residue, and woody biomass) and agricultural wastes (e.g., manure) with little or no available air and at moderate temperatures (Lehmann 2007). Because of the physical and chemical characterization, biochar contains different forms of amorphous carbon with abundant porosity and surface functional groups (C-O, C=O, COOH and OH, etc.), as well as minerals such as N, P, S, Ca, Mg, and K (Liu et al. 2015). More importantly, it has been increasingly reported that biochar has a strong adsorption affinity to various environmental contaminants due to the functional active sites, including heavy metals, organic compounds, and other inorganic oxyanions (Ashry et al. 2016, Wang et al. 2016a). For example, Ashry et al. (2016) tested biochar as a material for the fixation of U^{VI} from aqueous solutions. The batch experiments showed uranium adsorption on biochar was high over a wide range of pH values. Inyang et al. (2012) also reported that biochar displayed effective removal for different heavy metals (Pb^{2+}, Cu^{2+}, Ni^{2+} and Cd^{2+}). Besides, further adsorption investigations indicated the removal was mainly attributed to oxygen-containing groups of biochars (Uchimiya et al. 2011). However, understanding the interfacial mechanism between biochar and heavy metal ions in aquatic systems is still difficult due to data limitations and spectroscopic approaches. Therefore, the main objective of our research was to provide advanced insights regarding the interaction of Ni(II) with biochar by using macroscopic experiments. A series of environmental parameters such as pH, contact time, temperature, initial concentrations, and addition of humic acid (HA) or fulvic acid (FA), was also investigated by batch experiments.

MATERIALS AND METHODS

Materials and Chemicals

Biochars were produced from the pine needle and washed with deionized water several times to remove dust. After air-dried, ground, and filtered, the obtained litters via pyrolysis at 773 K for 12 h under oxygen-limited conditions. All solutions were prepared using 18 MΩ de-ionized water

(Milli-Q Gradient, Millipore, USA). The chemicals in all experiments were purchased in analytical grade and without further purification.

Batch Adsorption and Microscopic Experiments

The adsorption procedures of Ni(II) with biochars were investigated by mixing 0.1g.L^{-1} biochars and 15.0 mg.L^{-1} of initial Ni(II) concentration. The pH value was adjusted in the range of 2.0-10.5 by adding 0.001, 0.01, or 0.1 mol.L^{-1} $NaClO_4$ solutions, because ClO_4^- has little capacity to coordinate with metal ions (Cheng et al. 2015). The adsorption isotherms and thermodynamics were investigated at pH~6.5 with initial Ni(II) concentrations ranging from 5.0 to 18.0 mg.L^{-1} under the condition of 0.01 mol.L^{-1} $NaClO_4$ solutions. Then, the conical flasks with these mixtures were shaken in a thermostatic shaker for 24.0 h at 298.0 K to establish adsorption equilibrium. The samples were filtered out by a 0.45 μm membrane, the residual Ni(II) concentration in the solution was determined using a UV-vis spectrophotometer (UV-754 N shanghai, China) at 616.0 nm. The adsorption capacity of Nickel was calculated based on the initial and final aqueous concentrations. The reactive samples before and after reaction were characterized by scanning electron microscope (SEM), transmission electron microscope (TEM), Fourier transform infrared (FTIR) spectra analysis.

Characterization Approaches

The scanning electron microscopic (SEM) images were performed on a field emission scanning electron microscope (FEI-JSM 6320F). The Fourier transformed infrared (FTIR) spectra analysis was obtained using a Nexus 670 FTIR spectrometer (Thermo Nicolet, Madison) in the 4000-400 cm-1 wavenumber. The samples were equipped with a KBr beam splitter (KBr, FTIR grade). The background spectrum of KBr was also recorded under the same conditions. The surface area, pore volume (PV), and pore size distribution were determined by N2 Brunauer-Emmett-Teller (BET) adsorption-desorption at 77 K using Micromeritics ASAP 2010 equipment. The zeta potentials of the samples were measured with a Nanosizer ZS instrument (Malvern Instrument Co., UK) at room temperature.

RESULTS AND DISCUSSION

Characterization of Biochar

The morphological structure of obtained biochar was characterized by SEM, TEM, FTIR, BET surface area, pore volume

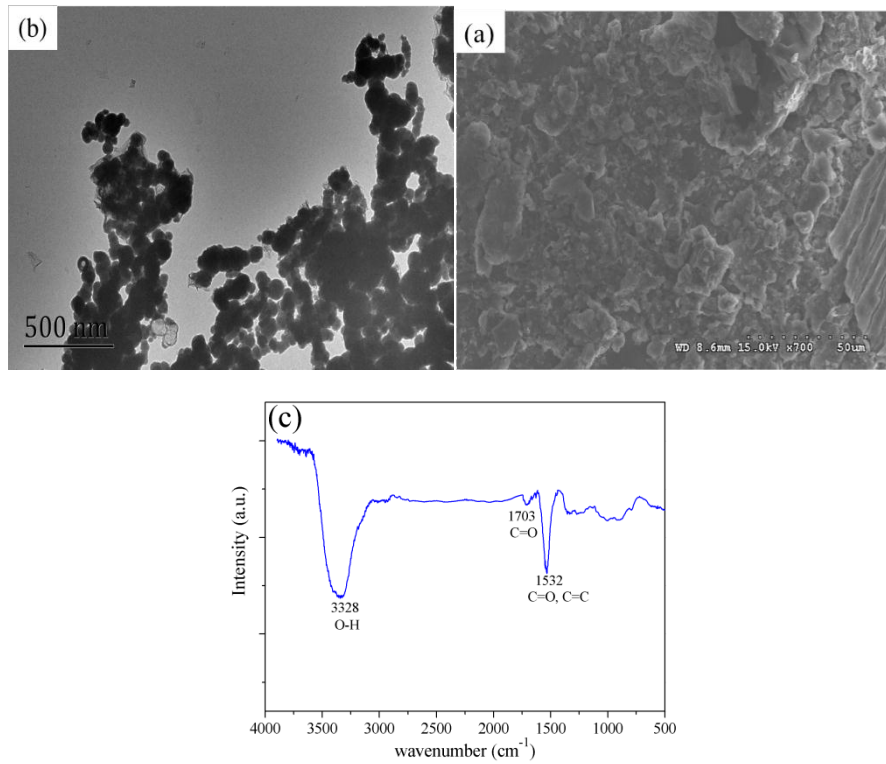

Fig. 1: The characterization of the biochar: (a) SEM; (b) TEM; (c) FTIR.

(PV), and pore size distribution (Fig. 1). The SEM image (Fig. 1a) and the high-resolution TEM image (Fig. 1b) both revealed an amorphous structure of carbon particles, indicating that the pine needles had been carbonized. FTIR spectra provided additional evidence of surface groups, as shown in Fig. 1c. The broadband at ~3328 cm^{-1} was assigned to the stretching mode of hydroxyl involved in hydrogen bonds or from interlayer water molecules, the peak that appeared at ~1703 cm^{-1} was due to C=O in the carboxyl group, and the band at 1532 cm^{-1} represented contribution from the vibration of C=O or C=C groups. Because of the large number of oxygen/carbon-containing functional groups on the surface, the adsorption capacity can be considerably increased. This is because surface OH and COOH groups of biochar interact with the metals *via* hydrogen bonding and complexation (Uchimiya et al. 2012). The value of pH at the point of zero charges (pH_{PZC}) for biochar was 6.5.

Effect of pH and Ionic Strength

The sorption of Ni(II) on biochars as a function of pH under different $NaClO_4$ concentrations was shown in Fig. 2. The outer-sphere surface complexation is more vulnerable to ionic strength variations, whereas the inner-sphere surface complexation with covalent bonding is unaffected by ionic strength variations (Jin et al. 2015). Besides, ClO_4^- does not form complexes with the concomitant metal ions in the solution. As a result, the ionic strength impact was useful in comparing and analyzing the role of ionic strength fluctuation. As shown in Fig. 2a, the sorption capacities increase with increasing pH from 2.0 to 7.0, while revealing no significant difference for 0.001-0.1 $mol.L^{-1}$ $NaClO_4$ concentrations, which demonstrated the inner-sphere surface complexation dominated the sorption. Correspondingly, the adsorption capacities tend to be stable and reach saturation under high alkaline conditions (herein, pH>8), which is similar to the sorption trend of other reported adsorbents for heavy metals (Ding et al. 2016). The phenomenon is mainly attributed to the formation of hydroxide precipitates. The sorption of Ni(II) was also studied under different pH conditions in Fig. 2b. It is seen that Ni(II) sorption increases at elevated pH. Zeta potentials showed that the pH_{ZPC} decreased with the increase of pH (Fig. 3), indicating the possible formation of the negatively-charged inner-sphere complexes (Pena et al. 2006).

Kinetic Study

The kinetics of Ni sorption and the impacts of silicate on Ni uptake onto biochar are shown in Fig. 4. Four different kinetic models including first-order, pseudo-second-order, intraparticle diffusion, and Elovich models are used to fit the experimental data. The equations of the models can be described as follows:

$$\ln(q_e - q_t) = \ln q_e - k_1 t$$

$$\frac{t}{q_t} = \frac{1}{k_2 q_e^{\,2}} + \frac{t}{q_e}$$

$$q_t = k_i t^{0.5}$$

$$q_t = \beta \ln(\alpha\beta) + \beta \ln t$$

Where q_e and q_t are the amount of adsorption of Ni(II) at equilibrium and at time t (min), k_1(min^{-1}) and k_2(min^{-1}) are the rate constant of adsorption, *ki* is the intraparticle diffusion rate ($mg.g.min^{-0.5}$), and α and β are the initial adsorption rate ($mg.g.min^{-1}$) and desorption constant ($g.mg^{-1}$).

The results of fitting experimental data are presented in Table 1. It is noticed from the correlation coefficient (R^2) that the pseudo-second-order equation is the most suitable for the description of adsorption kinetics of Ni(II) on biochar.

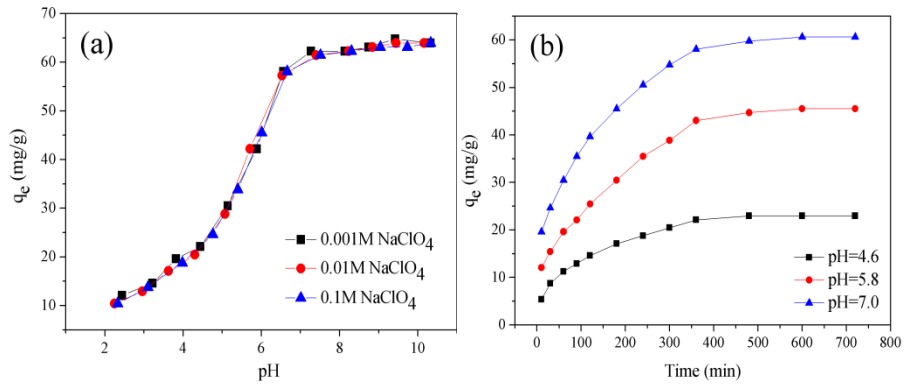

Fig. 2: Effect of ionic strength and pH: (a) Sorption of Ni(II) on biochar as a function of pH in different $NaClO_4$ concentrations; (b) Sorption of Ni(II) on biochar under various pH conditions, $m.V^{-1}$=0.1 $g.L^{-1}$, T = 293 K, $C_{(Ni)initial}$ = 15 $mg.L^{-1}$.

Table 1: Kinetic parameters and regression coefficients (R^2) for the four kinetic models.

pH	$q_{e,exp}$ [mg.g^{-1}]	Pseudo-first order			Pseudo-second order			Intraparticle diffusion		Elovich		
		k_1 ×10^{-2}	$q_{e,cal}$	R^2	k_2 ×10^{-2}	$q_{e,cal}$	R^2	k_i [mg.g.min$^{-0.5}$]	R^2	α	β	R^2
4.6	22.96	0.56	16.51	0.936	3.32	25.51	0.994	5.97	0.917	3.03	4.64	0.972
5.8	45.54	0.68	42.43	0.975	1.25	51.81	0.987	12.32	0.948	1.27	9.24	0.928
7.0	60.59	0.72	48.15	0.981	1.46	66.22	0.998	14.56	0.925	1.92	11.20	0.957

Similar results of pseudo-second-order kinetics trends in this study were observed in previous reports (Wang et al. 2016b, Zhu et al. 2016), which suggest the prevailing behavior over the whole range of the process is chemisorption. The intraparticle diffusion model is commonly used to comprehensively analyze the adsorption kinetics and to assess the importance of diffusion during the adsorption process (Guo et al. 2016). The model curves of q_t and $t^{0.5}$ have a non-linear relationship over the entire time range and can be divided into two stages without passing through the origin, indicating the mechanism for both surface adsorption as well as intraparticle diffusion.

Sorption Isotherms and Thermodynamic Analysis

Fig. 5 showed Ni(II) sorption isotherms on biochar at 293, 313, and 333K. The equation of Langmuir and Freundlich models could be expressed as follows:

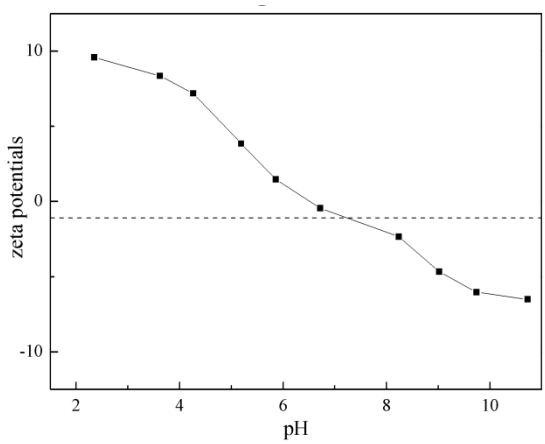

Fig. 3: Zeta potentials of biochar.

$$q_e = \frac{q_m K_L C_e}{1 + K_L C_e}$$

$$q_e = K_F C_e^{\,n}$$

Where C_e is the equilibrium concentration (mg.L^{-1}) and q_m is the maximum adsorption capacity of Ni(II), K_L is the Langmuir adsorption constant (L.mg^{-1}), and K_F (L.mg^{-1}) and n are the Freundlich constant corresponding to capacity and intensity of adsorption.

Table 2 listed the relative values calculated from the two models. The experimental data are well fitted by the Langmuir model than by the Freundlich model, indicating the sorption of Ni(II) on biochar is monolayer coverage. The calculated value of maximum adsorption capacity is 76.729 mg.g^{-1}, which is higher than granular activated carbon (39.5 mg.g^{-1}) (Kadirvelu et al. 2000). Besides, the sorption isotherm increased gradually with the increase of temperatures, which is shown the promotion with the reaction temperatures in the adsorption process. The thermodynamic parameters (ΔG^0, ΔH^0, and ΔS^0) for Ni(II) sorption on biochar can be calculated from the following equation and the results are presented in Table 3:

$$\Delta G^0 = -RT \ln K^0$$

$$\ln K^0 = \frac{\Delta S^0}{R} - \frac{\Delta H^0}{RT}$$

Where R is the ideal gas constant (8.314 J.mol.K^{-1}), K^0 is the sorption equilibrium constant, calculated by plotting $\ln K_d$ versus C_e (Fig. 6) and extrapolating the correlations of linear fits in Table 4.

Fig. 7 showed the linear relationship between $\ln K^0$ and 1/T, and the positive standard enthalpy change (ΔH^0) value

Table 2: The parameters for Langmuir and Freundlich isotherm.

T(K)	Langmuir			Freundlich		
	q_{max}(mg.g^{-1})	b (L.mg^{-1})	R^2	K_F(mg^{1-n}L^n.g^{-1})	n	R^2
293	76.729±1.061	0.300±0. 1	0.996	23.758±0.964	0.395±0.022	0.972
313	82.298±0.849	0.497±0. 8	0.994	35.311±0.891	0.299±0.0138	0.979
333	91.439±1.103	0.716±0. 8	0.986	47.08±0.733	0.24434±0.09	0.987

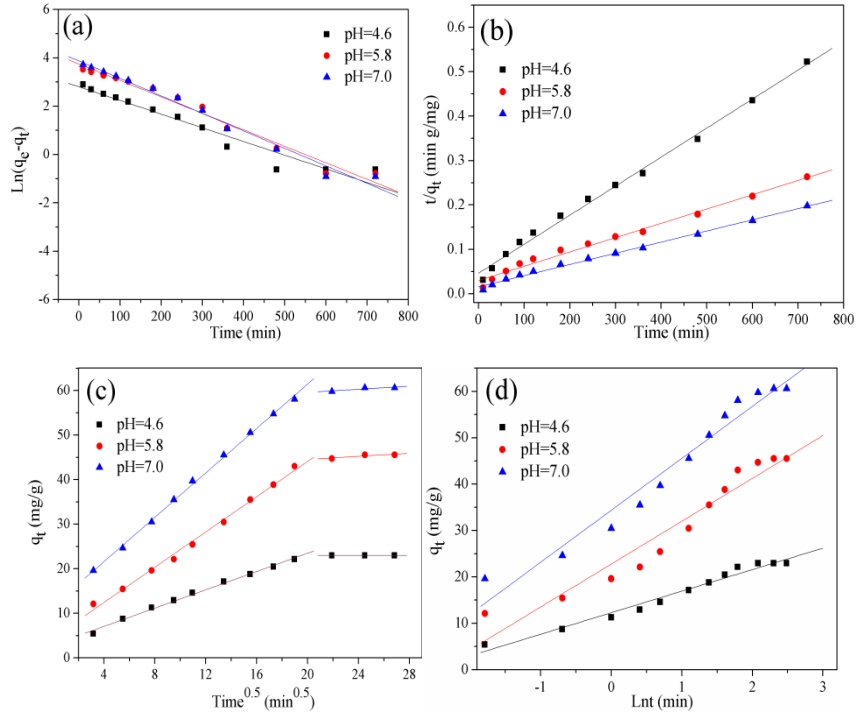

Fig. 4: Kinetic studies under various pH conditions: (a) first-order kinetics model; (b) Pseudo-second-order kinetics model; (c) Intraparticle diffusion model; (d) Elovich equation model. T = 293 K, m.V^{-1}=0.1g.L^{-1}, $C_{(Ni)\ initial}$ = 15 mg.L^{-1}, I=0.01 M $NaClO_4$.

represents the sorption of Ni(II) on biochar is an endothermic process. The standard free energy change (ΔG^0) is negative with the positive value of the standard entropy change (ΔS^0) indicating the spontaneous nature of the treatment process.

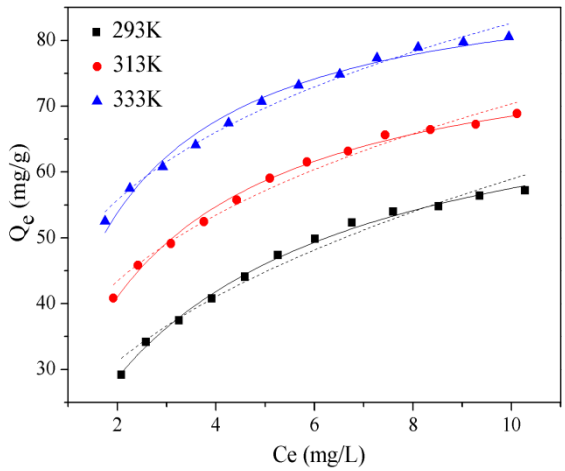

Fig. 5: Sorption isotherms of Ni(II) on biochar at different temperatures. m.V^{-1}= 0.1 g.L^{-1}, pH= 6.5, I=0.01 M $NaClO_4$. The solid lines are Langmuir model simulation, and the dashed lines are Freundlich model simulation.

Effect of HA and FA

In addition, natural organic matters (NOMs), including humic acid (HA) and fulvic acid (FA), contain functional groups such as carboxyl, amine, and phenolic, have also been known to strongly impact the sorption on biochars (Yang et al. 2016). Fig. 8 showed the pH dependence of Ni(II) adsorption on biochar under the condition of absence and presence of HA/FA. We can see that the removal of

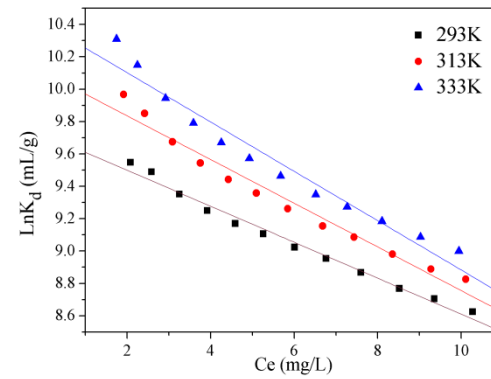

Fig. 6: Linear plots of $\ln K_d$ vs C_e for the sorption of Ni(II) on biochar at different temperatures. m.V^{-1}=0.1 g.L^{-1}, pH=6.5, I=0.01 M $NaClO_4$.

Table 3: Thermodynamic parameters for the sorption.

T (K)	ΔG_0 [kJ.mol^{-1}]	ΔH_0 [kJ.mol^{-1}]	ΔS_0 [J.mol.K^{-1}]
293	-23.683	13.9	128.3
313	-26.299		
333	-28.812		

Table 4: Constants of linear fit of ln*Kd* vs. *Ce* (ln*Kd* = A + B*Ce*).

T(K)	T[°C]	A	B	R
293	20	9.722±0.028	-0.111±0.0042	0.984
313	40	10.106±0.047	-0.13495±0.0075	0.967
333	60	10.407±0.062	-0.152±0.010	0.954

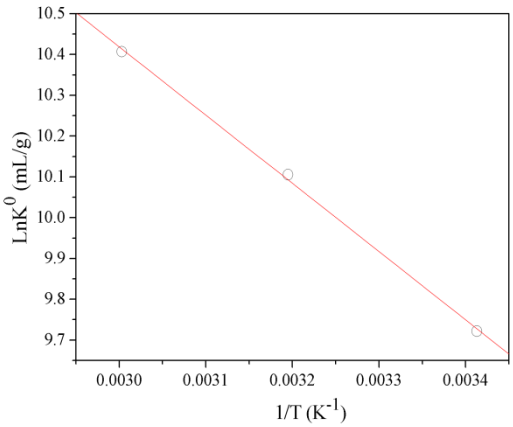

Fig. 7: Linear plot of lnK^0 vs 1/T for the sorption of Ni(II) on biochar at 293, 313, and 333K. m.V^{-1}=0.1 g.L^{-1}, pH=6.5, I=0.01 M $NaClO_4$.

Ni(II) on biochar was promoted significantly by adding HA/FA at pH<7 while inhibiting the reaction at pH>7. The NOMs have been recognized to have a strong complexation ability to metal ions by acting as a contaminant adsorbent (Uchimiya et al. 2010). As the pH rises, negatively charged HA/FA find it more difficult to bind to the negatively charged surface of the charcoal, and hence perform the opposite role. The adsorption curves for the impact of HA and FA have a comparable tendency, implying that the functional structures of HA and FA are similar (Sheng et al. 2014). Similar results are also demonstrated from the adsorption behaviors of Pb(II) on β-MnO_2 (Zhao et al. 2010).

Regeneration

The recycling of biochar for Ni(II) elimination was examined as a potential future practical application. Biochar was desorption tested by washing it numerous times with Milli-Q water and then drying it at 80°C for regeneration. At least six times, repeated experiments were carried out. The adsorption capacity of biochar for Ni(II) decreased slightly even after six rounds, indicating that biochar has strong reuse qualities in Ni(II) adsorption.

CONCLUSION

Based on the preceding discussion, biochars show to be available adsorbents for heavy metal uptake while taking into account the effects of pH, contact time, temperature, starting concentrations, and humic compounds. At low pH, outer-sphere surface complexes are thought to be converted into inner-sphere surface complexes, and surface precipitates occur on the biochar surface.

REFERENCES

Ashry, A., Bailey, E.H., Chenery, S.R.N. and Young, S.D. 2016. Kinetic study of time-dependent fixation of U^{VI} on biochar. J. Hazard. Mater., 320: 55-66.

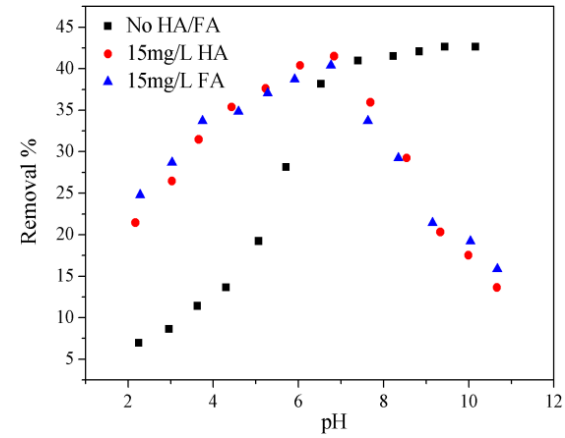

Fig. 8: Effect of HA/FA on the sorption of Ni(II). M.V^{-1}=0.1 g.L^{-1}, pH=6.5, I=0.01 M $NaClO_4$.

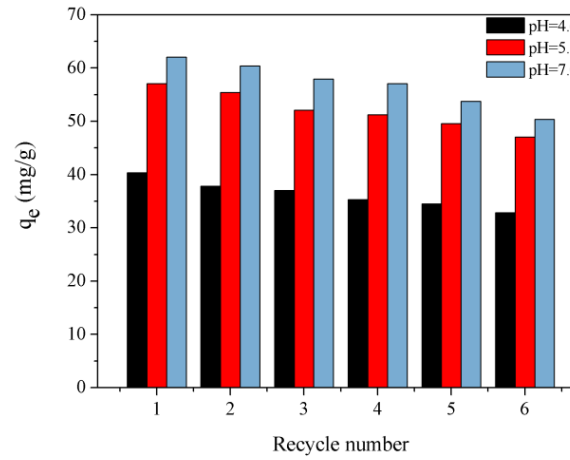

Fig. 9: Recycling of biochar for the removal of Ni(II). M.V^{-1}=0.1g.L^{-1}, pH=6.5, I=0.01M $NaClO_4$.

Cheng, W., Jin, Z., Ding, C. and Wang, M. 2015. Simultaneous sorption and reduction of U(VI) on magnetite-reduced graphene oxide composites investigated by microscopic, spectroscopic, and modeling techniques. RSC Adv., 5: 59677-59685.

Ding, C., Cheng, W., Wang, X., Wu, Z., Sun, Y., Chen, C., Wang, X. and Yu, S. 2016. Competitive sorption of Pb(II), Cu(II), and Ni(II) on carbonaceous nanofibers: A spectroscopic and modeling approach. J. Hazard. Mater., 313: 253-261.

Guo, X. Dong, H. Yang, C., Zhang, Q., Liao, C., Zha, F. and Gao, L. 2016. Application of goethite modified biochar for tylosin removal from aqueous solution. Colloids Surf. A, 502: 81-88.

Inyang, M., Gao, B., Yao, Y., Xue, Y., Zimmerman, A.R., Pullammanappallil, P. and Cao, X. 2012. Removal of heavy metals from aqueous solution by biochars derived from anaerobically digested biomass. Bioresour. Technol., 110: 50-56.

Jin, Z., Wang, X., Sun, Y., Ai, Y. and Wang, X. 2015. Adsorption of 4-n-nonylphenol and bisphenol-A on magnetic reduced graphene oxides: A combined experimental and theoretical studies. Environ. Sci. Technol., 49: 9168-9175.

Kadirvelu, K., Faur-Brasquet, C. and Le Cloirec, P. 2000. Removal of Cu(II), Pb(II), and Ni(II) by adsorption onto activated carbon cloths. Langmuir, 16: 8404-8409.

Lehmann, J. 2007. A handful of carbon. Nature, 447: 143-144.

Liu, W., Jiang, H. and Yu, H. 2015. Development of biochar-based functional materials: Toward a sustainable platform carbon material. Chem. Rev., 115: 12251-12285.

Malkoc, E. 2006. Ni(II) removal from aqueous solutions using cone biomass of thuja orientalis. J. Hazard. Mater., 137: 899-908.

Pena, M., Meng, X., Korfiatis, G.P. and Jing, C. 2006. Adsorption mechanism of arsenic on nanocrystalline titanium dioxide. Environ. Sci. Technol., 40: 1257-1262.

Sheng, G., Ye, L., Li, Y., Dong, H., Li, H., Gao, X. and Huang, Y. 2014. EXAFS study of the interfacial interaction of nickel(II) on titanate nanotubes: role of contact time, pH, and humic substances. Chem. Eng., J. 248: 71-78.

Uchimiya, M., Lima, I.M., Klasson, K.T. and Wartelle, L.H. 2010. Contaminant immobilization and nutrient release by biochar soil amendment: roles of natural organic matter. Chemosphere, 80: 935-940.

Uchimiya, M., Wartelle, L.H., Klasson, K.T., Fortier, C.A. and Lima, I.M. 2011. Influence of pyrolysis temperature on biochar property and function as a heavy metal sorbent in soil. J. Agric. Food Chem., 59: 2501-2510.

Uchimiya, M., Bannon, D.I. and Wartelle, L.H. 2012. Retention of heavy metals by carboxyl functional groups of biochars in small arms ranges soil. J. Agric. Food Chem., 60: 1798-1809.

Wang, Z., Shen, D., Shen, F. and Li, T. 2016a. Phosphate adsorption on lanthanum-loaded biochar. Chemosphere, 150: 1-7.

Wang, Y., Lu, H., Liu, Y. and Yang, S. 2016b. Ammonium citrate-modified biochar: an adsorbent for La(III) ions from aqueous solution. Colloids Surf. A, 509: 550-563.

Yang, Z., Kappler, A. and Jiang, J. 2016. Reducing capacities and distribution of redox-active functional groups in low molecular weight fractions of humic acids. Environ. Sci. Technol., 50: 12105-12113.

Zhao, D., Yang, X., Zhang, H., Chen, C. and Wang, X. 2010. Effect of environmental conditions on Pb(II) adsorption on β-MnO_2. Chem. Eng. J., 164: 49-55.

Zhu, N., Yan, T., Qiao, J. and Cao, H. 2016. Adsorption of arsenic, phosphorus, and chromium by bismuth impregnated biochar: Adsorption mechanism and depleted adsorbent utilization. Chemosphere, 164: 32-40.